Catalysis Science & Technology

Accepted Manuscript

Catalysis
Science &
Technology

rsc.li/catalysis

Volume 7
Number 2
21 January 2017
Pages 313–534

ISSN 2044-4761

ROYAL SOCIETY
OF CHEMISTRY

PAPER
Chaoqiu Chen, Yong Qin et al.
Highly dispersed Pt nanoparticles supported on carbon
nanotubes produced by atomic layer deposition for hydrogen
generation from hydrolysis of ammonia borane

This is an Accepted Manuscript, which has been through the Royal Society of Chemistry peer review process and has been accepted for publication.

Accepted Manuscripts are published online shortly after acceptance, before technical editing, formatting and proof reading. Using this free service, authors can make their results available to the community, in citable form, before we publish the edited article. We will replace this Accepted Manuscript with the edited and formatted Advance Article as soon as it is available.

You can find more information about Accepted Manuscripts in the Information for Authors.

ROYAL SOCIETY
OF CHEMISTRY

rsc.li/catalysis

Catalysis Science & Technology Accepted Manuscript

ARTICLE

Site-specific catalytic activities to facilitate solvent-free aerobic oxidation of cyclohexylamine to cyclohexanone oxime over highly efficient Nb-modified SBA-15 catalysts

Wei Ding, Haoyu Peng, Wenzhou Zhong*, Liqiu Mao*, Dulin Yin

The development of highly active and selective heterogeneous catalysts for efficient oxidation of cyclohexylamine to cyclohexanone oxime is a challenge associated with the highly sensitive nitrogen-center of cyclohexylamine. In this work, dispersed Nb oxide supported on SBA-15 catalysts are disclosed to efficiently catalyze selective oxidation of cyclohexylamine with high conversion (>75%) and selectivity (>84%) to cyclohexanone oxime by O_2 without any addition of solvent (TOF = 469.8 h^{-1}, based on the molar amount of Nb sites). The role of active-site structure identity is probed in dictating the site-specific catalytic activities with the help of different reaction and control conditions and multiple spectroscopic methods. Complementary to the experiments results, further poisoning tests (with KSCN or dehydroxylation reagents) and DFT computational studies clearly unveil that the surface exposed active centers toward activation of reactants are quite different: the surface –OH groups can catch NH_2 group from cyclohexylamine by forming a hydrogen bond and lead to a more facile cyclohexylamine oxidation to desired products, while the monomeric or oligomeric Nb sites with highly distorted structure play an key role in the dissociation of O_2 molecules beneficial for insertion of active oxygen species into cyclohexylamine. These catalysts exhibit not only satisfactory recyclability for cyclohexylamine oxidation, but also efficiently catalyze the aerobic oxidation of a wide range of amine under solvent-free conditions.

Introduction

Cyclohexanone oxime is one of the most important intermediates in chemical industry, particularly as a key precursor of ε-caprolactam for the polyester Nylon-6 production.[1,2] In 2012, the worldwide cyclohexanone oxime production capacity was approximately 560 million tons/year, and the demand is projected to grow at an annual rate of 2~3% in the next decade.[3] Currently, most methods of cyclohexanone oxime production involve the condensation of cyclohexanone with hydroxylamine sulfates as nitrogen source (Fig. 1). This conventional technology route, however, is via a multi-step process with low atom-efficiency (63%) and coproduces large volumes of salt waste.[4,5] So far, several new methods for the preparation of cyclohexanone oxime from cyclohexanone have been developed to minimize waste. Liquid-phase cyclohexanone ammoximation to cyclohexanone oxime with ammonia and H_2O_2 over TS-1 has achieved industrialization.[6,7] An attempt with the cheap O_2 as oxidant for ammoximation of cyclohexanone with ammonia has been examined using $Co^{II}Co^{III}AlPO-36$ catalysts.[8] However, the biggest challenge of these methods is the difficulty in obtaining cyclohexanone with 80% selectivity, which is usually supplied by aerobic cyclohexane oxidation with a low conversion of less than 5% by preventing the deep-oxidation.[9] Recently, a

interesting method has also been proposed that the transformation involves the hydrogenation of nitrobenzene or nitrocyclohexane with all the atoms (100%) needed to form the cyclohexanone oxime structure.[10,11] Alternatively, the use of cyclohexylamine as the feedstock to cyclohexanone oxime is particularly attractive route by compared with the conventional methods, as its significant advantages include easy availability and the elimination of the inorganic by-products. Cyclohexylamine can be widely obtained from benzene via nitrobenzene and aniline, nitrocyclohexane, cyclohexene or cyclohexanol. Particularly, this successful implementation in atomic-economy will provide a new green
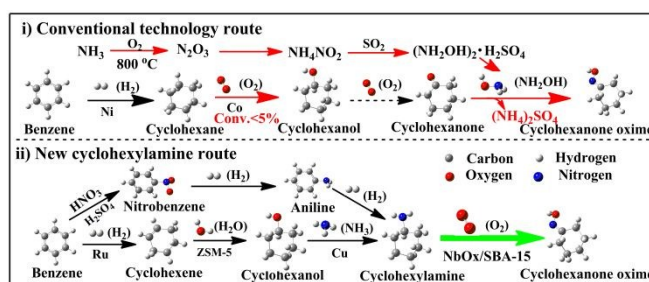

Fig. 1 Existing commercial hydroxylamine-based route (i) and alternative cyclohexylamine-based route (ii) for cyclohexanone oxime production.

dimension for the development of new cyclohexanone oxime preparation route with almost 100% theoretical atom from benzene via hydrogenation, hydrolysis, amination with NH_3 as nitrogen source and cyclohexylamine oxidation.

a. National & Local United Engineering Laboratory for New Petrochemical Materials &Fine Utilization of Resources, Hunan Normal University, Changsha 410081, P. R. China. E-mail: zwenz79@163.com, mlq1010@126.com; Tel: +86-731 88872576; Fax: +86-731-88872531

Although oxyfunctionalization of cyclohexylamine with industrial potential is of great importance throughout the chemical value-chain for the production of cyclohexanone oxime, they remain problematic transformations to achieve, both with respect to the selective formation of desired cyclohexanone oxime and the nature of the oxidizing species. This is just one example of how selective cyclohexylamine oxidation can offer interesting and attractive new opportunities. At present, various methods for the transformation of cyclohexylamine to cyclohexanone oxime are limited owing to the highly sensitive nitrogen-center of $-NH_2$ groups. Several oxidation procedures using stoichiometric oxidants such as Cr^{VI} salts, Dess-Martin, or tert-butyl hydroperoxide have been reported.[12,13] These processes, however, suffer from the formation of an equivalent amount of organic or toxic waste, which leads to low atom economy and environmental issues. Given an environmentally benign reduction byproduct (H_2O), catalytic oxidation of cyclohexyl-amine with H_2O_2 in the presence of TS-1 or heteropolyacid, gives cyclohexanone oxime, nitrocyclohexane and cyclohexanone.[14] Nevertheless, its cost is still prohibitive for less value-added cases.[12,15] As a result, a catalytic system using O_2 has been desired in view of environmental and economical aspects. Silica, γ-Al_2O_3, WO_3/Al_2O_3 or heteropolyacid are known to be capable of catalyzing vapor-phase aerobic oxidation of cyclohexylamine at higher temperature (>443 K) to give the corresponding oxime in low yields.[16-19] Recently, Ti-based catalysts are demonstrated to be efficient for aerobic oxidation of cyclohexylamine to oxime.[20,21] The reported method with employing an organic 1, 1-diphenyl-2-picrylhydrazyl catalyst and WO_3/Al_2O_3 cocatalyst in CH_3CN solvent is found to give oxime in high yields.[22] With regard to the synthesis of cyclohexanone oxime by aerobic cyclohexylamine oxidation, potentially practical and sustainable processes need to employ heterogeneous catalysis, especially in a solvent-free manner; however, this is extremely challenging to simultaneously achieve high activities and selectivities in such transformations.

In recent years, niobium-based materials have been quickly emerging as the effective catalysts in the field of heterogeneous catalysis. Owing to its uniform acidity and water tolerant properties, wide research activities are focused on acid-catalyzed reactions such as hydrolysis[23,24] and dehydration[25,26]. In addition, niobium materials also show the ability to release oxygen in active peroxo-niobium, either by treatment of H_2O_2 or on photo-irradiation, and act in oxidation of various substrates such as SO_2[27], alkenes[28], 5-hydroxymethylfurfural[29], thioethers[27] and alcohols[30]. Among these studies, however, the work on selective oxidation of amine to the corresponding oxime with O_2 as a cheaper oxidant over niobium-derived heterogeneous catalysts is still very scarce, possibly because Nb catalysts seem to afford a lower catalytic activity. Herein, we report the aerobic selective oxidation of cyclohexylamine to cyclohexanone oxime using niobium-based heterogeneous catalysts in a solvent-free system. By changing the preparation method to adjust the structure of niobium species and surface hydroxyl groups on the catalysts, the efficiency of cyclohexylamine oxidation to cyclohexanone oxime was optimized. The catalyst with Nb species in extra-framework portion prepared by impregnation showed a 75.2% cyclohexylamine conversion at 373 K, with a cyclohexanone oxime selectivity of 84.3%. Our Nb catalysts for turnover frequency (TOF=469.8 h^{-1}) outperform all W or Ti-based catalysts previously employed. The experimental and computational results show that selective site-specific adsorption-activation of Nb species and surface –OH groups takes place in the different reactants to promote the selective oxidation of cyclohexylamine.

Results and discussion

Characterization of the catalysts

ICP-AES analysis was used to determine the quantitative

Table 1 Textural property of the different samples.

Catalyst	S_{BET}[a] (m^2/g)	S^{ext} (m^2/g)	Pore size[b] (nm)	Pore volume (cm^3/g)	Nb, wt% as assumed	Nb, wt% ICP
SBA-15	668	648	5.87	1.02	-	-
Nb/SBA-15/1im	661	634	5.79	0.98	1.0	0.9
Nb/SBA-15/3im	576	557	5.41	0.86	3.0	2.8
Nb/SBA-15/5im	548	518	5.33	0.78	5.0	4.9
Nb/SBA-15/7im	527	509	5.16	0.76	7.0	6.8
Nb-SBA-15/3co	723	690	7.67	1.30	3.0	2.7

[a] BET surface area. [b] The pore-size distribution determined by the BJH method.

amount of Nb metals present in the samples and the results are shown in Table 1. The data clearly show that the amount of metals employed during the catalyst preparation are close to the expected values. N_2 adsorption/desorption isotherms characterise the difference between the prepared catalysts (Table 1 and Fig. S1). A wider hysteresis loop (characteristic of large-pore mesoporous solids[31]) is shifted to low relative pressure in the range of 0.54 and 0.80 with increasing Nb-loading amounts, suggesting a decrease in the pore size for the Nb/SBA-15/im samples. However, this effect is not

observed for Nb-SBA-15/3co prepared by co-condensation, which shows a hysteresis loop very similar to that of pristine SBA-15. Among the samples investigated, Nb-SBA-15/3co shows the highest specific surface area (S_{BET}, 723 m^2/g) with 1.30 cm^3/g total pore volume, whereas Nb/SBA-15/im samples show a lower S_{BET} (527 ~ 661 m^2/g) and total pore volume (0.76 ~ 0.98 cm^3/g) compared to the parent SBA-15. This behavior is in agreement with the fact that niobium species can be incorporated into the framework of SBA-15 with promoting the Si–O–Nb linkages for Nb-SBA-15/3co; a

regularly decrease in S_{BET} and total pore volumes for the Nb/SBA-15/im samples is attributed to the increase in the sample density after impregnation with the higher molecular weight Nb species.

Compared with the parent SBA-15 support, two less intense peaks between 1.64° and 1.85° in Low-angle XRD patterns provide evidence that the mesoporous structure remains intact after
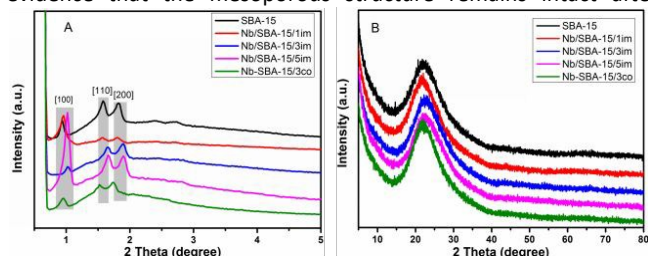

Fig. 2 Low-angle (A) and high-angle (B) XRD patterns of samples.

impregnation (Fig. 2A).[32] The positions of diffraction peaks for Nb/SBA-15/im samples are higher than those of SBA-15 support which testified that the ordering porous structure of SBA-15 was partly distorted after the impregnation of Nb species. In case of Nb-SBA-15/*3*co, all diffraction signals are shifted to lower values, which can be attributed to an increase in the unit cell parameter caused by the incorporation of Nb ions with larger ionic radius (0.64 Å) in the SBA-15 framework.[3] The characteristic reflections of crystalline niobium oxide (JCPDS card No. 00-007-0061) are not detected for any catalyst (Fig. 2B), which indicates that Nb ions are either well dispersed or attained an amorphous oligomeric form outside of the framework.

TEM images of the samples in Fig. 3 demonstrate the retention of the periodic structure, which shows a long range periodic structure and niobium oxide species encapsulated into the
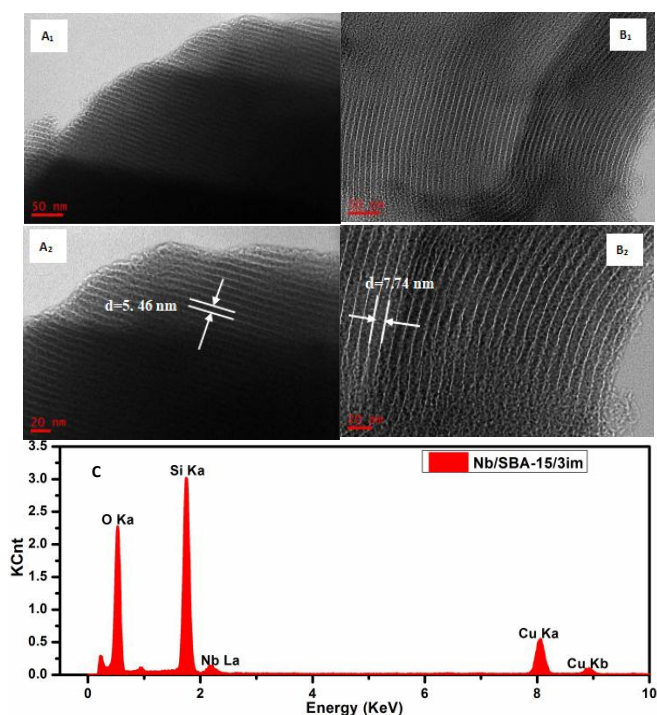

Fig. 3 TEM images of Nb/SBA-15/3im sample (A_1 and A_2) and Nb-SBA-15/3co sample (B_1 and B_2); X-ray spectroscopy (EDS) of Nb/SBA-15/3im sample (C).

framework or highly dispersed on surfaces of mesoporous silica. Further, uniform pores can also be observed from the Nb-SBA-15/*3*co sample, and their pore size is the larger (d=7.74 nm, 3B_2) compared to Nb/SBA-15/*3*im (5.46 nm, 3A_2), which is well agree with the average pore diameter from N_2 physisorption. This result reveals that the incorporation of more niobium oxide species into the framework for Nb-SBA-15/*3*co might be caused by co-condensation procedure. Based on the substrate diameters (<1.1 nm) by DFT calculation, the reaction is not controlled or limited by pore diffusion. Energy dispersive X-ray spectroscopy (EDS) of the Nb/SBA-15/*3*im sample displays the presence of niobium, oxygen, silicon and copper elements (Fig. 3C), and the presence of copper element is attributed to the conductive copper tape used in the EDS measurement.

Raman spectroscopy is employed to investigate the isolated NbO_4 information and extent of oligomer formation in networks of surface niobium oxides (Fig. 4A). Comparison with pure Nb_2O_5, similar bridging Nb–O–Nb bands at approximately 664 and 234 cm^{-1} are observed in Nb/SBA-15/im samples with high Nb content (>3%).[33] Meanwhile, some remarkable modifications of these signals with regard to broadness and position toward lower frequencies are also detected, which can be associated with the NbO_6 distortions for the phonon relaxation energy by alteration of the niobium structure.[34] The new peak appears at approximately 462 cm^{-1} assigned to the bridging Nb–O–Nb–O–Si sites, confirming the presence of agglomerized extra framework niobium species. Meanwhile, all Nb-loaded samples possess a Raman band at about 967 cm^{-1}, which is related to symmetric stretching of terminal Nb=O bonds on the surface due to highly dispersed Nb species.[35] In the 790-810 cm^{-1} region, tetrahedral NbO_4 shows its major Raman bands,[36] and the intensity is higher in the spectrum of Nb-SBA-15/*3*co sample. Therefore, two types of surface niobium species are most likely present in the samples: one is the surface monomeric or oligomeric NbO_6 species, another one is the NbO_4 species.

FT-IR spectra of Nb-modified SBA-15 samples show a sharp and weak peak is observed at ca. 3736 cm^{-1} (Fig. 4B), which is characteristic of terminal –OH bonded to distorted NbO_6 species present on the surface.[37] Comparison with pure silica support, two band intensities at 3459 and 1630 cm^{-1} for Nb/SBA-15/im samples decrease upon the loading of small amounts of niobia, showing a drastic decrease of the amount of silanol groups, indicating that the loading of Nb species on SBA-15 consumes surface Si–OH. With further increasing the Nb-loading amount, an increase in absorption, however, is observed likely due to hydrogen-bonding interactions between silanols and more neighboring Nb-OH groups. In contrast, these peak intensities for Nb/SBA-15/3co

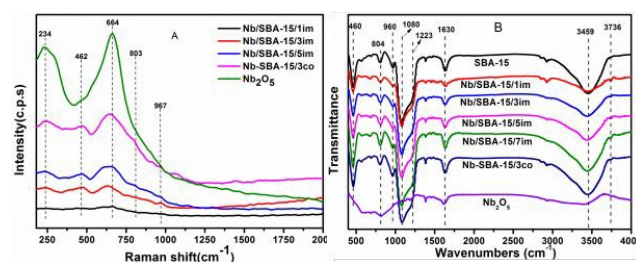Fig.4 UV-Raman spectra (A) and FT-IR spectra (B) of samples.

prepared by co-condensation, however, are about the same as those of the silica support. In addition, the band at 960 cm^{-1} is due to a Si–O vibrational mode perturbed by the presence of metal ions in a neighboring position. A similar band has been observed for titanosilicates, which is assigned to surface titanyl species Ti–O or tetrahedral TiO$_4$ units.[38] Thus, we assign the band at 960 cm^{-1} in the IR spectra of Nb-modified samples to the presence of Si–O–Nb structure by a [SiO$_4$] unit bonded to a niobium ion (O$_3$Si–O–NbO$_3$).[39]

UV-Vis spectra of the Nb-modified catalysts are obtained with SBA-15 and Nb$_2$O$_5$ as references (Fig. 5A). Various Nb/SBA-15/im samples show a band around 210 nm associated with local Nb–O–Si bonds in monomeric [NbO$_4$] tetrahedral units,[40] which is also observed for the as-synthesized Nb/SBA-15/3co. This indicates that part of niobium species introduced by impregnation is incorporated into the zeolite framework, which is consistent with the results of Liu et al.[41] Comparison with pure Nb$_2$O$_5$, the broad band centered around 250 nm with a tail extending from 270 nm can be assigned to distorted NbO$_6$ octahedra, and the intensity increases with increasing the doping of Nb content. This can be related to a wider distribution of monomeric Nb structural units, with the presence of a greater amount of more oligomeric NbO$_6$ species in the high Nb-loaded samples.[42] The Nb/SBA-15/3co sample prepared by co-condensation can be also observed similar absorptions at 210 and 270 nm, but the intensities are much lower in the same content. Thus, Nb/SBA-15/im samples prepared by impregnation is highly dispersed on the surface of the siliceous support, which is in well agreement with the XPS and X-ray fluorescence studies that XPS and bulk Nb/Si atomic ratios are very similar for Nb/SBA-15/im samples.

The qualitative and quantitative study on the niobia presence at the surfaces are carried out by X-ray photoelectron spectroscopy (XPS), and are shown in Table S1 and Fig. 5B. XPS
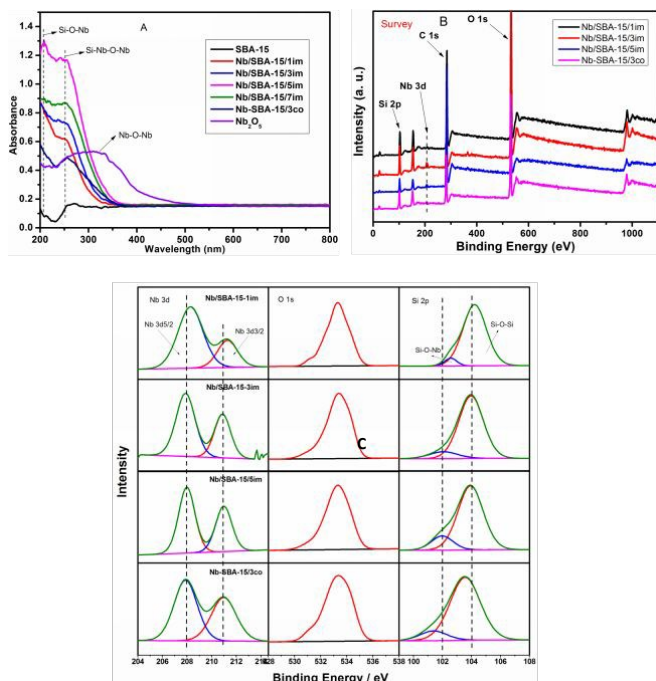

Fig. 5 UV-Vis spectra (A) of samples; Survey spectrum of samples (B) and XPS spectra of Nb 3d, O 1s and Si 2p of samples (C).

surveys for all Nb-modified samples clearly show the presence of Si, Nb, O and trace amounts of adventitious C from pure SBA-15. XPS analysis for Nb3d spectra revealed spin-orbit doublet peaks centred at ca. 208.0 eV (3d5/2) and ca. 211.0 eV (3d3/2) demonstrating the presence of Nb^{5+} in an oxide surrounding.[43] However, the shift toward higher values (208.3 eV) than that typical of Nb$_2$O$_5$ species (207.0 eV) has been attributed to the high dispersion of niobium oxides on the support and to the change in the Nb coordination by formation of Nb–O–Si or or Si–O–Nb–O–Nb linkages. Moreover, the binding energy of Nb 3d follows a decreased trend towards those observed for crystalline Nb$_2$O$_5$ with increasing the Nb-loading amount, as shown in Fig. 5C. This can contain contributions arising from different niobium species such as a spot of small oligomer on the surface of catalysts,[44] which is in agreement with what already observed by Raman and UV-Vis spectra. From quantitative XPS results, the surface Nb molar concentrations can be determined from the surface Nb/Si ratios. Table S1 shows the comparison between the surface Nb/Si atomic ratio values as determined by using XPS and those corresponding to the bulk atomic ratio by using X-ray fluorescence techniques. The XPS and bulk Nb/Si atomic ratios are very similar for Nb/SBA-15/7im prepared by impregnation. However, when the Nb species loading is prepared by co-condensation, the surface Nb/Si atomic ratio notably decreases with respect to that of the bulk Nb/Si for the Nb/SBA-15/3co. This confirms the high ability of the impregnation method to accommodate host phases, as niobium oxide, at the surface of the guest silica matrix. Niobium oxide is well-dispersed over the surface of the support as previously reported.[45] The O1s lineshape region (Fig. 5C) for all the Nb-loaded catalysts show an almost symmetric peak in the region 532.9–533.1 eV, close to the value observed for O^{2-} of SBA-15 support (533.0 eV),[46] which evidenced the presence of homogeneously dispersed Nb species on the surface of the mesoporous support.

Pyridine adsorption *in-situ* FTIR spectra is collected for the Nb/SBA-15/im and Nb/SBA-15/3co samples in the region of 1630~1400 cm^{-1} (Fig. 6). In the case of Nb/SBA-15/1im samples, the bands at 1446 and 1597 cm^{-1} dominate (Fig. 6A), which is attributable to the pyridine adsorbed via a weak hydrogen-bonding on surface hydroxyl groups (e.g., Si–OH or Nb–OH).[47] Meanwhile, these peak intensities increased with increasing the Nb content up to 3% and decreased with a further increase, which is attributable to the concentration distribution of surface OH groups. On the other hand, several weak peaks for adsorbed pyridine are also observed at 1577, 1544 and 1491 cm^{-1}. The band at 1577 cm^{-1} arises from adsorbed pyridine on Lewis acid sites;[40] absorbance features at 1544 cm^{-1} is assignable to pyridinium ions originated from the Nb–OH–Nb in polymerized Nb species,[47,48] and peak intensities keep progressive increase with increasing Nb$_2$O$_5$ content. The band at 1491 cm^{-1} rises from the presence of Si–OH–Nb or Nb–OH–Nb sites in which the pyridine is thought to bond simultaneously to Lewis and Brønsted acid sites.[49] Compared to Nb/SBA-15/3im, significant increases of peak intensities at 1444 and 1598 cm^{-1} are observed for Nb/SBA-15/3co prepared by co-condensation (Fig. 6A), indicating more surface Si–OH groups. Further, IR spectra of Nb/SBA-15/3im is recorded after evacuation at various temperatures. As shown in Fig. 6B, the peaks
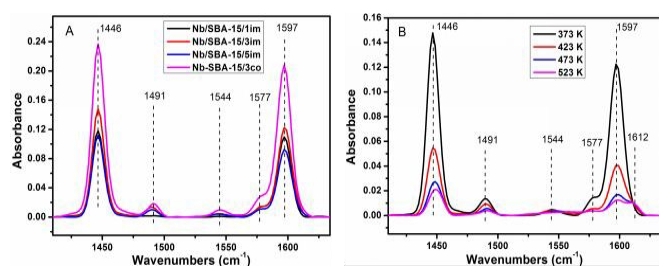
Fig. 6 Pyridine adsorption in-situ FTIR spectra of samples (A) and pyridine adsorption in-situ FTIR spectra of Nb/SBA-15/3im after evacuation at various temperatures.

attributable to the pyridine adsorbed via a weak hydrogen-bonding obviously decreased after evacuation at 423 K, which is attributable to a reduction in the number of the surface OH groups. The bands attributable to weak Lewis-bound pyridine (1576 cm^{-1}) diminish at a further increase in evacuation temperature (473 K), while a new band at 1610 cm^{-1} origined from strong Lewis-bounded pyridine appears. The strong Lewis-bounded reactants is unfavorable to the selectivity of desired products from the point of view of catalysis.

Catalytic activities

Selective aerobic oxidation of cyclohexylamine to cyclohexanone oxime catalyzed by the various Nb-based catalysts under solvent-free conditions is investigated on cyclohexylamine, known to be highly sensitive to auto-oxidation with main formation of nitro-compound and ketone-derived products. The catalytic results compared with the corresponding Nb$_2$O$_5$ and SBA-15 supports are shown in Table 2. Blank experiment without any catalysts shows that a remarkably low cyclohexylamine conversion (5.7%) with only small amounts of cyclohexanone oxime (34.2%) is obtained as a result of the thermal auto-oxidation process (entry 1). Meanwhile, the bulk Nb$_2$O$_5$ is active for the cyclohexylamine oxidation and gives good oxime selectivity (>73%) along with the main cyclohexyl-cyclohexylidene-amine by-product (13.2%), whereas a low cyclohexylamine conversion of 15.9% is observed under study (entry 3). One can generally believe that O$_2$ dissociates on Nb sites by transferring charge density from Nb sites to the vacant π* molecular orbital of adsorbed O$_2$,[50,51] which is produced concomitantly and thereby generates active oxygen species for the initiation of oxidation reaction. Interesting, its reactivity is significantly improved by the introduction of SBA-15 as supports; in striking contrast, about 75.2% of the cyclohexylamine is converted with Nb/SBA-15/3im under the same conditions, and the higher selectivity to cyclohexanone oxime (84.3%) is achieved along with the main nitrocyclohexane by-product (entry 9). This finding strongly supports that the supported niobium-sites structure with a different coordination environment is responsible for the enhanced catalytic activity in the selective oxidation process. Actually, we also tested the activity of a sample of mechanically mixed Nb$_2$O$_5$ and SBA-15 (3 wt% of SBA-15), and the conversion is only one-third of that of Nb/SBA-15/3im (not shown), with producing a quantity of nitrocyclohexane by-products. Thus, the differently loaded Nb/SBA-15/im catalysts are tested for their activity and selectivity in the selective oxidation of cyclohexylamine with the aim to study the influence of niobium-site structures on the catalytic performance, and the

turnover frequency (TOF) values for cyclohexylamine conversion based on niobium sites on catalyst are calculated. Generally, cyclohexylamine conversion increases with increasing niobium loading up to 5 wt.% Nb; at higher loadings cyclohexylamine conversion keeps nearly constant (entries 8-11). The TOF of the lowest content Nb species is very high (740.1 h^{-1}), and TOFs in oxidation reactions strongly decrease with increasing Nb loading. As already discussed in the preceding characterization section, the monomeric or oligomeric niobium species become progressively polymerized with increasing surface coverage. Therefore, one can conclude that monomeric or oligomeric niobium species are intrinsically more active than their high agglomerated counterparts. Meanwhile, the total selectivity of the main cyclohexyl-cyclohexylidene-amine and cyclohexanone by-products over Nb/SBA-15/1im is 17.5% and higher than the selectivity of 14.0% achieved over Nb/SBA-15/7im catalysts with higher niobium loading, which indicates that further hydrolysis of cyclohexanone oxime is catalyzed by Lewis acidic sites. This observation can be explained by the stronger Lewis acidity of monomeric or oligomeric niobium-sites compared to higher aggregated ones. On the contrary, the relative selectivity of nitrocyclohexane by-product increases with an increase in the niobium loading, which suggests that higher aggregated niobium species show a higher catalytic activity toward further oxidation of cyclohexanone oxime to nitrocyclohexane.

To elucidate whether the niobium-sites linked to the silica surface is a key structure in determining the catalytic performances, we compare the catalytic activity and selectivity of the reaction performed on the Nb sites incorporated in the framework for Nb/SBA-15/3co containing the same moles of niobium. Relatively lower catalytic activity (conversion and TOFs), however, is obtained under similar conditions (entry 12). This can be a result of the change in surface speciation of Nb/SBA-15/3co, and Nb incorporated in the framework is relatively less reactive for oxidation process. To gain a further insight into the roles of the Nb species toward the oxygen activation, two sets of poisoning experiments have been carried out with KSCN involved in the reactions, which is thought that the metal sites would deactivate for the O$_2$ activation due to the strong affinity of SCN$^-$ ions to Nb metals by the formation of highly stable metal-ligand compounds.[52,53] One of the experiments is investigated with the addition of KSCN (15 equiv. relative to Nb) into the catalytic systems over the Nb$_2$O$_5$ catalyst, the cyclohexylamine conversion significantly decreases from 15.9% to 1.1%; another cyclohexylamine oxidation to cyclohexanone oxime over Nb/SBA-15/3im shows a similar trend in KSCN-based poisoning experiment. This phenomenon reveals that only Nb sites on the catalyst surface can be strongly coordinated by SCN$^-$ ions and affect their electron donating ability to the vacant π* molecular orbital of adsorbed O$_2$. As a result, Nb sites on the catalyst surface provide a direct catalytic site for the activation of O$_2$, as generally accepted for O$_2$ dissociation on transition metals such as Au, Pt and Ru in the literature.[54,55]
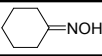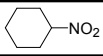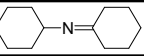
In addition, it should be considered if −OH groups present on the surface of Nb-loaded SBA-15 samples are in sufficient amount to account for the high activity. First, pure SBA-15 support is generally considered a catalytically inactive solid with composed

of Si–O–Si and Si–OH species, which is investigated as a possible reference (entry 2). Interesting, a notable catalytic activity (12.4%) is observed under similar conditions, but cyclohexanone oxime selectivity is remarkably lower (53.7%) over this support. Obviously, this catalytic activity is related to the surface Si–OH groups of support. Cyclohexylamine possesses electronegative nitrogen due to its –NH$_2$ groups and therefore it is easily adsorbed on –OH sites by formation of hydrogen bonds,[56] resulting in a lower reaction energy barrier for the oxidation of cyclohexylamine. This result is further confirmed by the fact that both Nb/MCM-41/im and Nb/Silicate-1/im at the same Nb loading containing higher concentration of surface –OH groups exhibit also high conversion of cyclohexylamine to cyclohexanone oxime (entries 6 and 7). Nb-loaded Al$_2$O$_3$ also exhibits a relatively high catalytic activity; nevertheless, the selectivity to cyclohexanone oxime is lower than that of Nb-loaded silica (entry 5). One can argue from the product distribution, further hydrolysis of cyclohexanone oxime occurs along with oxidation process, which is catalyzed by the stronger Lewis acidity sites from the Al–O–Al or Al–O–Nb structure of Nb/Al$_2$O$_3$/im due to the strong interaction between Nb^{5+} or Al^{3+} and the C=N bond of oxime. In addition, the changes on the surface of the catalyst with regard to catalytic activity are also confirmed by the experiment with the use of Nb/C/im having no surface Si–OH groups, in which the poor

activity and selectivity (cyclohexylamine conversion, 18.1%; cyclohexanone oxime selectivity, 50.7%) are observed under the same reaction conditions. Meanwhile, the surface-OHs of Nb/SBA-15/3im are dehydroxylated using a trimethylsilylation or triphenylsilylation agent and the formation of oxime decreases, which supports this conclusion (entries 13, 14). Thus, the presence of hydroxyl groups is essential to observe the enhanced catalytic activity for cyclohexylamine oxidation when using niobium containing catalysts.

Based on above catalysis, one has to consider the changes of the –OH active sites taking place on the catalyst surface in determining the catalytic performances. The best performing catalyst, Nb/SBA-15/3im, is dehydrated at 423, 623, and 823 K respectively and the corresponding catalytic activities are also investigated under the same conditions. The Nb/SBA-15/3im catalyst dehydrated at 423 K gives a higher cyclohexylamine conversion (83.7%) and than that of untreated Nb/SBA-15/3im catalyst (entry 15). One can conclude that the removal of weakly adsorbed bulk water to release more Si–OH and Nb–OH groups at 423 K can improve the accessibility of cyclohexylamine to surface active sites. Opposing this result, a dehydration of temperature at 623 K affords a relatively low cyclohexylamine conversion (54.2%)

Table 2 Selective aerobic oxidation of cyclohexylamine catalyzed by the various Nb-based catalysts under solvent-free conditions[a].

Entry	Catalyst	Conv.(%)[b]	Selectivity (%)[c]					Yield/% (oxime)	TOF.[d] (h^{-1})
			=O	=NOH	-NO$_2$	-N=	Others[e]		
1	None	5.7	4.7	34.2	27.0	19.9	14.2	1.9	-
2	SBA-15	12.4	21.2	53.7	18.2	0.6	6.3	6.7	-
3	Nb$_2$O$_5$	15.9	5.0	73.6	3.3	13.2	4.9	11.7	99.3
4	Nb/C/3im	18.1	11.2	50.7	13.0	11.3	13.8	9.2	113.1
5	Nb/γ-Al$_2$O$_3$/3im	36.2	23.8	37.1	8.7	27.8	2.6	13.4	226.2
6	Nb/MCM-41/3im	60.8	4.7	74.6	3.7	15.9	1.1	45.4	379.5
7	Nb/Silicate-1/3im	51.9	5.4	68.4	15.2	9.1	1.9	35.5	324.3
8	Nb/SBA-15/1im	39.5	3.2	78.5	1.8	14.3	2.2	31.0	740.1
9	Nb/SBA-15/3im	75.2	2.7	84.3	9.7	1.3	2.0	63.4	469.8
10	Nb/SBA-15/5im	79.0	8.6	61.1	26.1	1.2	3.0	48.3	296.7
11	Nb/SBA-15/7im	80.1	12.9	31.8	50.3	1.1	3.9	25.5	214.5
12	Nb-SBA-15/3co	64.3	7.3	67.4	20.7	1.8	2.8	43.3	401.7
13[f]	Nb/SBA-15/3im	21.5	3.7	80.9	11.7	2.0	1.7	17.4	134.4
14[f]	Nb/SBA-15/3im	34.1	6.0	69.9	21.2	0.8	2.1	23.8	213.0
15[g]	Nb/SBA-15/3im	83.7	2.1	81.7	12.6	1.0	2.6	68.4	531.6
16[g]	Nb/SBA-15/3im	54.2	5.4	75.1	14.3	2.8	2.4	40.7	338.4
17[g]	Nb/SBA-15/3im	38.7	4.4	68.0	21.4	4.0	2.2	26.3	241.8
18[h]	Nb$_2$O$_5$	1.1	2.8	18.9	7.2	70.1	1.0	0.2	6.9
19[h]	Nb/SBA-15/3im	42.3	3.1	79.9	8.9	5.0	3.1	33.8	264.3
20[i]	Nb/SBA-15/3im	13.7	5.9	32.7	47.3	5.9	8.2	4.5	85.6
21[j]	Nb/SBA-15/3im	4.6	16.1	49.8	12.5	14.4	7.2	2.3	28.7

[a] All reactions were done with 0.10 g of catalyst, 10.0 g (101.0 mmol) of cyclohexylamine, 0.8 MPa O$_2$, 373 K, time (5 h). [b] Conversion (%) based on substrate = {1–[(concentration of substrate left after reaction) × (initial concentration of substrate)−1]} × 100; [c] Product selectivity = content of this product/(adding cyclohexylamine amount (mmol)-the amount of cyclohexylamine recovered (mmol)) × 100%. [d] Turnover frequency (TOF): number of moles of cyclohexylamine converted per mole of catalyst (Number in parentheses is based on number of moles of Nb sites only). [e] Others: cyclohexanol, cyclohexene, N, N'-dicyclohexyl-hydrazine, N-cyclohexyl-N'-cyclohexylidene-hydrazine and small amounts of unidentified products. [f] Using the dehydroxylated Nb/SBA-15/3im by a trimethylsilylation (entry13) or triphenylsilylation (entry14) agent. [g] Nb/SBA-15/3im is dehydrated at 423 K (entry15), 623 K (entry16), and 823 K (entry17) respectively. [h] Using KSCN (15 equiv. relative to Nb) as a poisoning additive for Nb species in the oxidation system. [i] Using the alkaline Nb/SBA-15/3im by 0.5% NaOH treatment. [j] Addition of 5 mol% 2,6-di-tert-butyl-p-cresol as a free radical scavenger.

ARTICLE

and 75.1% cyclohexanone oxime selectivity (entry 16), which is expected to explain by the loss of part –OH groups for the activation of cyclohexylamine (Fig. S2). A similar effect is observed at very high dehydration temperatures (823 K) with only 38.7% cyclohexylamine conversion and 68% cyclohexanone oxime selectivity (entry 17).
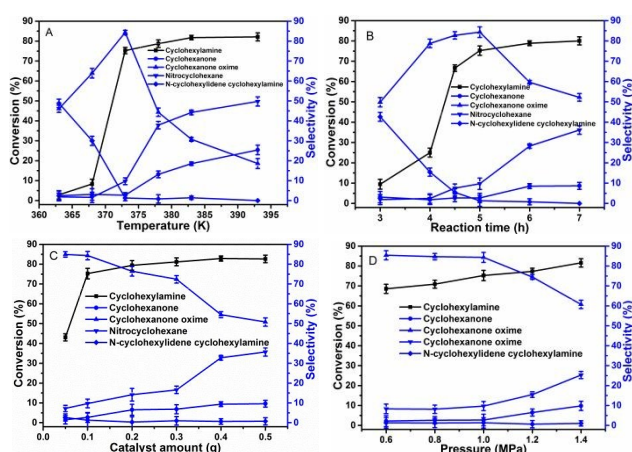

Fig. 7 Effect of the temperature (A), reaction time (B), catalyst amount (C) and pressure (D) on the conversion of cyclohexylamine and cyclohexanone, cyclohexanone oxime, nitrocyclohexane, cyclohexyl-cyclohexylidene-amine and others selectivity over the synthesized Nb/SBA-15/3im catalyst.

In order to further understand the product distribution in the cyclohexylamine oxidation under solvent-free conditions, the catalytic performance of Nb/SBA-15/3im is further optimized by tuning reaction parameters (Fig. 7). The catalyst displays a very low catalytic activity (8.3%) with only 63.9% oxime selectivity at 368 K, but with increasing temperature from 368 to 373 K the conversion of cyclohexylamine rapidly increased to 75.2% (Fig. 7A). These results indicate that the higher reaction temperature favors the activation of oxygen molecule by niobium species as well as the formation of dissociative chemisorptions of cyclohexylamine by surface hydroxyl groups in the first reaction step. Meanwhile, the cyclohexanone oxime selectivity also increases sharply from 63.9% to 84.3%, which suggests that a decrease in the strength of adsorption of cyclohexanone oxime on the surface of catalyst due to the temperature increase leads to avoid further hydrolysis of cyclohexanone oxime catalyzed by Lewis acidic sites. Further increase in the reaction temperature (378~393K) leads to a remarkable increase in the ability to further oxidation of cyclohexanone oxime (cyclohexanone and nitrocyclohexane are the main product with the total selectivity of about 70%, which is caused by the higher oxidizing ability of the Nb sites), while this effect is less pronounced for cyclohexylamine conversion. The effect of the reaction time on the aerobic oxidation of cyclohexylamine is investigated (Fig. 7B), the conversion to cyclohexanone oxime is very low (9.5%) in the

beginning of the reaction. After 3 h, the conversion and cyclohexanone oxime selectivity increases progressively, indicating the presence of reaction induction period. A possible explanation for this phenomenon is attributed to a radical-type autoxidation process. Further increasing the reaction time (up to 6 h) causes the decline of oxime selectivity, implying the occurrence of over-oxidation. In order to further find out the radical-based intermediates in oxidation process, we take aliquots of the sample at regular intervals and analysed them by iodometric titration, and no hydroperoxide is detected. One can suggest that the possible hydroperoxide intermediates under reaction conditions are quickly transformed into more stable products. Fig. 8C presents that initially the conversion of cyclohexylamine increases slightly with the catalyst weight in the range 0.05~0.4 g, whereas cyclohexylamine conversion is not affected much by further addition of catalyst. Obviously, a concomitant decrease in the selectivity of cyclohexanone oxime product with an increase in the amount of catalysts, implies a direct participation of Nb species in catalyst in the rate-determining step of the oxime over-oxidation. Finally, an increase of reaction pressure from 0.6 MPa to 1.4 MPa results in a slightly enhancement of the cyclohexylamine conversion to 81.6% with the oxime selectivity of 56.7% (Fig. 7D). This phenomenon is attributed to an enhancement of oxygen solubility making more oxygen accessible in the reaction medium.

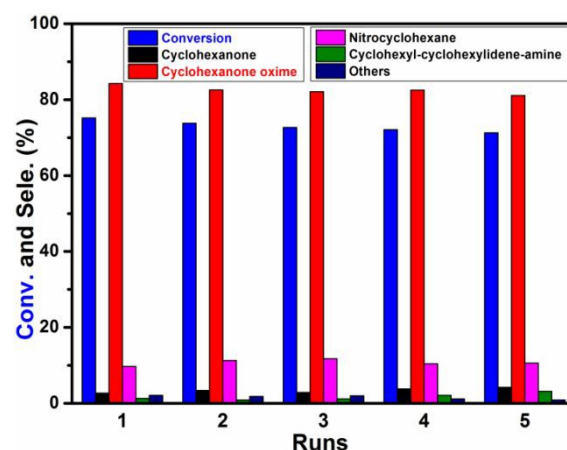From the context of a 'green' approach, the solvent-free

Fig. 8 Recyclability tests of Nb/SBA-15/3im catalyst for the cyclohexylamine oxidation. All reactions were carried out with 0.10 g of catalyst, 10 g of cyclohexylamine (101.0 mmol), 0.8 MPa O_2, 373 K, time (5 h).

oxidation of cyclohexylamine to cyclohexanone oxime with dioxygen is performed for a reused Nb/SBA-15/3im catalyst under the same reaction conditions. After simple separation and washed thoroughly with ethanol for three times, Nb/SBA-15/3im catalyst

after five successive oxidation cycles do not lead to any significant decline in its efficiency in terms of conversion and oxime selectivity (Fig. 8), demonstrating its good recyclability and deactivation resistance. Owing to Nb-based catalyst with water tolerant properties, some similar phenomenons are also reported for aqueous acid-catalyzed processes and epoxidation of alkene with H_2O_2,[24] proving to be truly of a heterogeneous nature. Furthermore, after completion of each run, the solid catalyst is removed from the reaction mixture by hot-filtration. The resulting filtrate is independently analyzed by ICP-AES analysis for the presence of niobium, and no niobium ions are present in the filtrate. The UV-Vis and FT-IR profiles of the spent catalysts are very similar to those of the fresh catalysts, as shown in Fig. S3. As a result, its catalytic efficiency and recyclability will make this Nb-based catalyst attractive for both fundamental research and practical applications. To prove the universality of this catalytic oxidation system based on Nb/SBA-15/3im, the selective oxidation of several other types of amines is further examined under solvent-free conditions, and the results are listed in Table 3. Similar to cyclohexylamine, alicyclic primary amines containing hydrogen atoms at the α-carbon such as cyclopentylamine and cycloheptanamine give the high catalytic activity and >73% oxime selectivity (entries 9 and 11). However, aliphatic primary amine
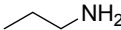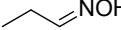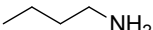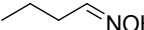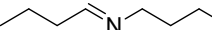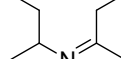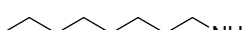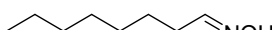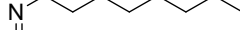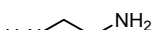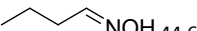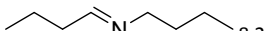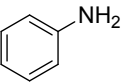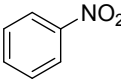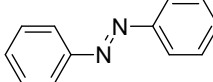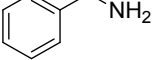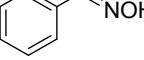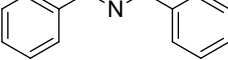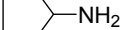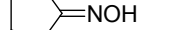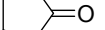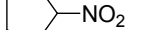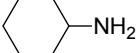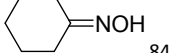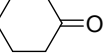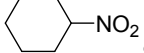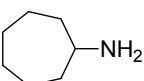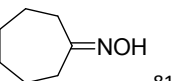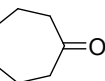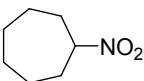
such as 1-propylamine, 1-butylamine 2-butylamine, n-octylamine and benzyl amine with a hydrogen atom at the α-carbon can also be converted into the corresponding oxime, but given the poor selectivity for oxime (entries 1-4 and 8). These aliphatic primary amines can experience oxidative coupling to their corresponding imines with high selectivity, implying that the different structures can affect the product distribution due to the existence of an electronic effect in this reaction. Meanwhile, the primary diamines such as ethanediamine are much less accessible owing to the intrinsic self-coupling properties of the substrates, unfortunately no oxime selectivity is observed with a low conversion rate of diamine (entry 5). However, the primary amine lacking hydrogen atoms at the α-carbon such as aniline can not be oxidized to the corresponding oxime or imine (entry 7), implying that the α-hydrogen is involved in the oxime or imine formation. Meanwhile, the aerobic oxidation of secondary amines such as di-n-butylamine with hydrogen atoms at the α-carbon gives the 1-butanone oxime with 44.6% selectivity over Nb/SBA-15/3im catalyst (entry 6).

DFT treatments of oxygen and cyclohexylamine adsorption-activation

Selective site-specific adsorption-activation takes place as the

ARTICLE

Table 3 Selective aerobic oxidation of various amines catalyzed by the 3% Nb/SBA-15 catalysts under solvent-free conditions[a].

Entry	Substrate	Conv. (%)[b]	Selectivity (%)[c]			TOF.[d] (h^{-1})
1	~NH$_2$ (propylamine)	13.5	NOH 26.1	N= 69.8		141.5
2	~NH$_2$ (butylamine)	24.0	NOH 53.3	N= 41.4		203.3
3	NH$_2$ (sec-butylamine)	11.0	NOH 30.8	N= 69.2		93.2
4	~NH$_2$ (octylamine)	9.2	NOH 10.3	N= 79.1		44.1
5	H$_2$N~NH$_2$ (ethylenediamine)	2.3	pyrazine 100			23.7
6	~NH~ (dibutylamine)	15.5	NOH 44.6	N= 8.2		74.4
7	aniline-NH$_2$	1.1	NO$_2$ 20.9	N=N 79.1		7.3
8	benzyl-NH$_2$	83.5	NOH 16.8	N= 83.2		482.7
9	cyclopentyl-NH$_2$	77.9	=NOH 73.3	=O 7.6	NO$_2$ 12.8	566.7
10	cyclohexyl-NH$_2$	75.2	=NOH 84.3	=O 2.7	NO$_2$ 9.7	469.7
11	cycloheptyl-NH$_2$	64.3	=NOH 81.5	=O 3.8	NO$_2$ 10.4	351.8

[a] All reactions were done with 0.10 g of catalyst, 10.0 g of reactant, 0.8 MPa O$_2$, 373 K, time (5 h). [b] Conversion (%) based on substrate = {1−[(concentration of substrate left after reaction) × (initial concentration of substrate)$^{-1}$]} × 100. [c] Main product selectivity = content of this product/(adding reactant amount (mmol)-the amount of reactant recovered (mmol)) × 100%. [d] Turnover frequency (TOF): number of moles of substrate converted per mole of catalyst. Number in parentheses is based on number of moles of Nb sites only.

first elementary step of catalytic processes, which consists of a link between the reactants and the catalytic active centers.[57,58] Based on the experimental examination of surface active centers by Raman, XPS, UV-vis and FT-IR methods, three possible types of active structures have been imagined (Fig. S4), in which the monomeric Nb species is grafted onto SBA-15 surface (a), or incorporated into the framework of SBA-15 (b) and dimeric Nb species (as an oligomeric model) is grafted onto SBA-15 surface (c). In these optimized structure models, the framework Nb=O bond lengths are 1.732~1.736 Å, which agrees well with EXAFS measurements of Nb=O bond lengths in the Nb species (1.73± 0.02 Å).[59] Similar findings have also been obtained by DFT calculations on Nb species.[60-62] To get insight about how the different Nb structures can activate oxygen, the interactions between O$_2$ and the Nb sites are optimized in Fig. 9. First, O$_2$ adsorbed on the monomeric (a-o) or dimeric (c-o) Nb sites grafted onto SBA-15 surface with a distance of 3.365 Å or 2.803 Å between Nb and O$_2$, is shorter than these of the O$_2$ adsorbed on the Nb sites (b-o) incorporated into the framework (3.400 Å). Second, the monomeric (a-o) or dimeric (c-o) Nb sites grafted onto SBA-15 surface shows a higher adsorption energies (E(ads)) of O$_2$ (12.1 kJ/mol, 14.5 kJ/mol) in comparison to the corresponding values for the Nb sites (b-o) incorporated into the framework (10.8 kJ/mol). This suggests that the surface Nb sites strengthened the O$_2$ adsorption and made the adsorbed O$_2$ easier to be activated.
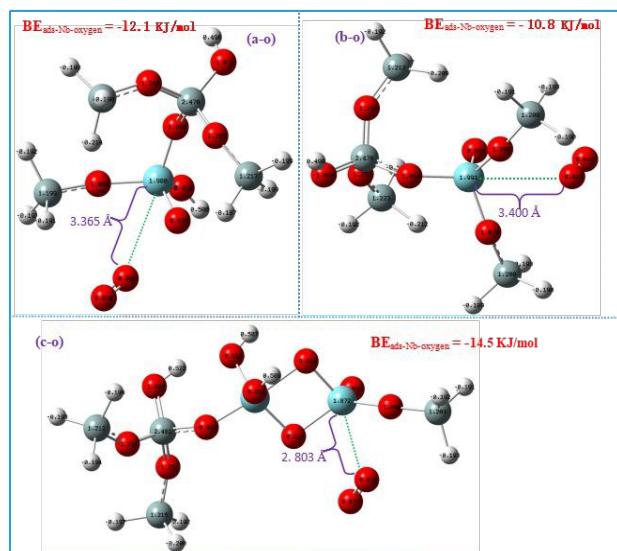
Fig. 9 Suggested simple models and electronic structure of optimized models for the isolated Nb species grafted onto SBA-15 surface (a-o), Nb species incorporated in the framework of SBA-15 (b-o) or oligomeric Nb species grafted onto SBA-15 surface (c-o) with the interactions between O₂ and the redox Nb sites. :Nb, :Si, :O, :H

Furthermore, the activation of O₂ in our case can be reflected by the change of number of electron transfer.[63] The NBO charge and molecular orbital analysis shows that the electron transferring occurs from one oxygen atom to another oxygen atom for adsorbed O₂, which caused by the surface Nb sites compared with the NBO charge free O₂ (0.000 e, Fig. S5 and S6). Owing to the electrophilic mechanism of the oxidation process, the lower electron density of the reactive center (O atom) is more likely to insert into the N–H bond.

To realize more clearly the different activities of Si–OH and Nb–OH for the activation of cyclohexylamine (models a-n1 and a-n2, Fig. 10), the basic geometric and electronic properties of active sites with adsorbed cyclohexylamine are investigated. Upon adsorption of cyclohexylamine, the calculated O–H bond length of active sites increases (Fig. 10 and Fig. S4) and the O–H bond length in Nb–OH is larger than that in Si–OH. Actually, this increase of O–H bond length is accompanied by a shortening in the formed N⋯H hydrogen-bonding length between the nitrogen of –NH₂ groups and the –OH, and consequently denotes a stronger tendency to transfer the electron on that site. This is in good agreement with results obtained by the computational adsorption energies: the adsorption energy is about 85.8 kJ/mol more stable for adsorption on the Nb–OH sites than on the Si–OH sites (76.3 kJ/mol). Due to the change in charge distribution around the N atom, the N–H bond in the adsorbed cyclohexylamine complex is significantly elongated (1.017 Å), compared to the free cyclohexylamine molecule (computational d_{N-H}=1.016 Å, Fig. S5). Therefore, a cleavage of the weak N–H bond of cyclohexylamine occurs easily over the coordinated nitrogen atom with the –OH site (particularly

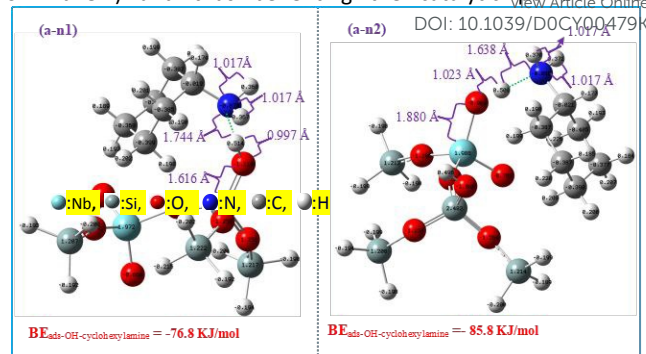for Nb–OH) and thus benefiting the catalytic performance.

Fig. 10 Suggested simple models and electronic structure of optimized models for the isolated Nb species grafted onto SBA-15 surface with the interactions between cyclohexylamine and the acidic Si-OH sites (a-n1) or Nb-OH sites (a-n2).

Reaction mechanism

Cyclohexylamine conversion to cyclohexanone oxime involves several key elementary steps, and each elementary step is thought to be catalyzed by a certain type of functional active sites (Fig. 11). The active Nb species and –OH groups in the present bifunctional Nb/SBA-15 catalysts mainly exist as site-specific catalytic centers toward the activation of different reactants. Combining the insights provided by preceding results, cyclohexylamine can be dissociatively chemisorbed on the –OH groups by hydrogen bonds. Meanwhile, dissociatively chemisorbed cyclohexylamine is dehydrated at reaction temperature. This can be confirmed by the following facts: (i) the reactivity of dehydroxylated Nb/SBA-15 or SBA-15 is decreased remarkably; (ii) the changes in activity are consistent with the observed surface hydroxyl-site contents by the dehydration temperature; (iii) the formation of cyclohexanone oxime strongly depends on the types of catalyst supports. Actually, this is also similar to the previous reports that pure silica shows reactivity for gas-phase cyclohexylamine oxidation at high temperature (>443 K).[18,19] Furthermore, DFT calculation reveals that the N–H bond for adsorbed cyclohexylamine by hydroxyl-sites is elongated from 1.016 Å to 1.017 Å, which can facilitate insertation of oxygen species with electrophilic property.

On the other hand, molecular oxygen can be selective chemisorbed on the dispersed Nb sites to form probably O²⁻ superoxo radical species, favoring the selective oxidation of cyclohexylamine. To verify the evidence for the formation of such radicals, a free radical scavenger (5 mol% 2,6-di-tert-butyl-p-cresol) was added (Table 2, entry 21). It was found that the radical scavenger had a strong inhibitory effect on the cyclohexylamine oxidation. In addition, our DFT calculations confirm that molecular oxygen can be dissociated on Nb sites, which is thought to be produced concomitantly and thereby generates active oxygen species by transferring charge density from metal to the vacant π* molecular orbital of adsorbed oxygen. This evidence is in line with our experimental studies that the poisoning additive (KSCN) for Nb species has a strong inhibitory effect on the cyclohexylamine reaction and therefore occurs by an active oxygen-based mechanism. Further per analogy to Nb-based catalyst,[61] experimental and theoretical studies have found that the proposed oxygen chemisorption species over Nb sites is very probable. Therefore, the active oxygen species are inserted into
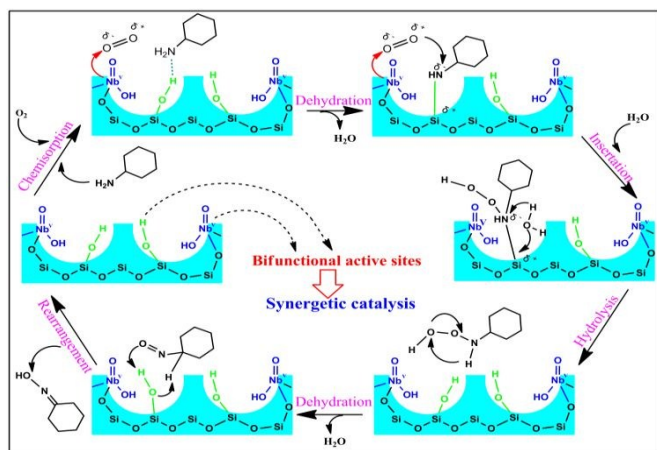
Fig. 11 Possible synergistic mechanism for the oxidation of cyclohexylamine with O_2 over the Nb-modified SBA-15 catalysts.

adsorbed amine to form absorbed amino peroxide, which further reacts with H_2O by the hydrolysis of Si–N bond to leave the catalyst surface and the recovery of the –OH groups. The formed free amino peroxide in our system is decomposed rapidly to form intermediate nitrosocyclohexane, in agreement with the results presented by Corma et al., who showed that it is possible to form nitroso compound directly.[64] If nitrosocyclohexane comes in contact with a Brønsted acid site, it can be quickly isomerized to cyclohexanone oxime which is released in the reaction medium.[19] This can be confirmed by poisoning experimental studies that the alkaline Nb/SBA-15/3im catalyst by 0.5% NaOH treatment gave the poor selectivity for oxime (Table 2, entry 20). Actually, a effective promotion of reaction rate is also obtained for amine oxidation with the acid-treated catalyst. As the coexistence of active oxygen species from Nb-based catalytic site, nitrosocyclohexane can also react with active oxygen species to form nitrocyclohexane by-products. Therefore, this underlines the importance of having strong Brønsted acid sites available at the catalyst surface (than weak Lewis acid sites). Thus, two different types of surface active sites should be well balanced to suppress formation of unwanted by-products.

Conclusions

In conclusion, we present the first green examples of Nb-modified mesoporous SBA-15 catalysts for selective oxidation of various amines using O_2 under solvent-free conditions. Particularly, the aerobic selective oxidation of cyclohexylamine into cyclohexanone oxime is thoroughly studied in order to get more insight into the structure-property correlation and mechanism for the oxidation of amine. The best Nb/SBA-15 catalyst with a 3% niobium content exhibits superior catalytic performance (TOF = 469.8 h^{-1}), achieving 75% cyclohexylamine conversion and 84% cyclohexanone oxime selectivity at 373 K. The results, obtained from the comprehensive experimental studies involving the characterization, detection, reaction of the different amines and reaction conditions have demonstrated that the surface dispersed Nb species and hydroxyl groups are identified as catalytic active sites for cyclohexylamine. The dispersed Nb species mainly catalyzed the activation of O_2 to active oxygen species, which is essential for the selective oxidation of cyclohexylamine. Both the activity and selectivity strongly depend on the exposed surface

hydroxyl groups of Nb/SBA-15 catalysts. This new dual active center model with site-specific catalytic activities, which has been validated by our experimental measurements and computational results, may provide a new avenue for unraveling the chemical properties of various metal-modified bifunctional catalysts.

Experimental

Catalyst preparation

Pure SBA-15 was synthesized according to literature[65] with Pluronic P123 triblock-co-polymer ($EO_{20}PO_{70}EO_{20}$). Reactant mixtures consisted of tetraethyl orthosilicate (TEOS), Pluronic P123, hydrochloric acid, and deionized H_2O with the molar ratio: 1 SiO_2 : 0.005 Pluronic P123 : 1.45 HCl : 124 H_2O. After the dissolving of Pluronic P123 in 1M hydrochloric acid solution, TEOS was added dropwise under stirring. The obtained mixture was continuously stirred at 313 K for 24 h and transferred into a Teflon-lined stainless steel autoclave and heated without any stirring at 373 K for 24 h. The solid product was filtered, washed with deionized water, dried at 373 K for 12 h and calcined at 823 K for 8 h to remove $EO_{20}PO_{70}EO_{20}$.

Method 1: Nb-loaded catalysts (Nb/SBA-15) were prepared by the aqueous impregnation method employing $NbCl_5$ as a precursor. The prepared SBA-15 (2 g) was poured into the ethanol solution of $NbCl_5$ to give 3 wt.% niobium (0.032 mol%) in the final product. After stirring at room temperature for 12 h, 9.0 mL deionized H_2O were slowly added to the mixture and vigorously stirred for 6 h and continually stirred for another 24 h. The impregnated sample was allowed to evaporate slowly at 383 K until dry sample was obtained. The 1wt.% (0.011 mol%), 5 wt.% (0.054 mol%) and 7 wt.% (0.075 mol%) Nb-loading samples were prepared by an identical procedure. The final samples contained 1, 3, 5, and 7 mass % of Nb (Nb/SBA-15/xim, with x representing the Nb mass %).

Method 2: Nb-incorporated SBA-15 molecular sieves (Nb-SBA-15) were prepared by co-condensation method with 3 mass % (0.032 mol%) of Nb (Nb-SBA-15/xco, with x representing the Nb mass %).[32] $NbCl_5$ was used as a niobium source with addition of hydrochloric acid. In this preparation method, an amount of $NbCl_5$ was first dissolved in 140 mL ultrapure H_2O, followed by the addition of 4 g $EO_{20}PO_{70}EO_{20}$ template. After dissolution of the template, 9.0 mL (40.7 mmol) of TEOS were added and stirred at 313 K for 24 h. The obtained suspension was placed into a Teflon-lined stainless steel autoclave and heated without the stirring at 373 K for 24 h. Then, the solid was filtered, washed and air dried at room temperature. The dried materials were air-calcined at 823 K for 8 h at a ramp rate of 10 K.

Characterization techniques

The crystalline phases of powers were characterized by a Bruker D8 ADVANCE diffractometer operated at 40 kV and 40 mA, using CuKα radiation with a wavelength of 1.542 Å. Particle size and morphological properties of samples were done using scanning obtained on a Hitachi S-4800 microscope, while the TEM images were collected using a

ARTICLE

JEOL 2010 field emission gun at 200 kV accelerating voltage. The near surface compositions of Nb and Si species in the synthesized solids were determined using an energy dispersive X-ray spectroscopy (EDS) equipped in the electron microscope JEOL-JSM-6400. The BET surface area and porosity of samples were obtained by N_2 adsorption at 77 K on a Tristar 3000 sorptometer. Prior to the tests, the samples were degassed at 473 K under vacuum until a final pressure of 1×10^{-5} Torr was reached. Raman spectra were obtained for solids on an inVia Raman microscope using the excitation wavelength from a laser at 325 nm. Framework infrared spectra of samples in KBr pellets were recorded at room temperature on an AVATAR 370 Thermo Nicolet spectrophotometer with a resolution of 2 cm^{-1}. UV/Vis diffuse-reflectance spectra were conducted on a Varian-Cary 5000 spectrometer with an integrating-sphere attachment using $BaSO_4$ as a reference to assess the nature of Nb species. The concentrations of Brønsted and Lewis sites in materials were determined by the infrared spectra of adsorbed pyridine using a custom-built transmission cell coupled to a Fourier transform infrared (FT-IR) spectrometer (Bruker, Tensor 37) with a liquid-N_2-cooled HgCdTe detector. The powders were pressed binder-free into self-supporting wafers with a density of 4.0~11.0 mg cm^{-2}. Prior to the adsorption of pyridine the samples were activated 'in situ' by overnight evacuation at 573 K. Pyridine was admitted at 373 K for 1 h in order to reach adsorption equilibrium, followed by degassing at different temperatures for 0.5 h, and then the IR spectrum was measured at 373 K. The surface electronic states were analyzed by X-ray photoelectron spectroscopy (XPS, Axis Ultra, Kratos Analytical Ltd.) with Al Ka radiation (1486.7 eV). Binding energies were referenced to the C_{1S} peak at 284.8 eV, and fit XPS software was used for curve fitting. Bulk elemental analysis was carried out with Inductive CouplePlasma Atomic Emission Spectroscopy (ICP-AES) on a spectroflame D (Spectro Analytic Instrument).

DFT calculations

On the basis of the experimental results, we chose the smallest geometrical structures with active Nb sites and surface hydroxyl groups as catalyst surface models for computation in this work, which provides a straightforward link between theory and experiment. In our system, Gaussian 09 program package was applied to perform our density functional theory (DFT) calculations using the B3LYP hybrid functional with tight self-consistent field (SCF) convergence and ultrafine integration grids.[66] The dispersion corrections were described by "Empirical Dispersion = GD3".[67] The 6-311++(d, p) basis set was adopted for the C, H, O, and N atoms, and the Nb atoms adopted the valence basis functional (LANL2DZ).[56,68] Natural bond orbital (NBO) analyses were performed using the NBO 6.0 program to gain insight into the natural charge distribution and bonding patterns for all the structures. In these models, the unsaturated bonds are saturated by hydrogen atoms. Vibrational frequencies were calculated for all obtained structures to confirm that they corresponded to the energy minima and obtained zero point vibrational energy (ZPE) corrections to the electronic energies.

The binding energies of oxygen or cyclohexylamine adsorbates on the catalyst surfaces with different active sites (BE_{ads}) were calculated by eq (1) : $BE_{ads}= E_{adsorbate+surface} -(E_{adsorbate} + E_{surface})$, in which $E_{adsorbate+surface}$ represented the total energy of the adsorbate interacting with the active sites of the catalyst, while $E_{adsorbate}$ and $E_{surface}$ were the energy of for the adsorbates in the gas phase and the bare catalyst surface respectively. One can do this by considering that there are two different adsorption sites on the surface for oxygen or cyclohexylamine, with energies $E_{ads-Nb-oxygen}$ and $E_{ads-OH-cyclohexylamine}$, each one can be calculated from equation (1).

Cyclohexylamine selective oxidation reaction

The catalytic selective oxidation of cyclohexylamine with molecular oxygen in the absence of solvent was carried out in a Teflon-lined stainless steel autoclave of 100 cm^3 capacity with a magnetical stirring. Typically, 10.0 g of cyclohexylamine (101.0 mmol) was mixed with 0.1 g of Nb/SBA-15 catalyst and then raised to the desired temperature (373 K). Then, oxygen was charged into the reactor to the desired pressure (0.8 MPa) and reaction was started by adjusting stirrer speed to 600 rpm. After reaction, the reactor was quickly cooled down and then depressurized carefully. The products were dissolved in ethanol and the solid catalyst was separated from aqueous phase by filtration. The mixtures were quantitatively analyzed by a gas chromatography (GC, Agilent 6890N, 30 m × 0.32 mm × 0.50 μm DB-17 polysiloxane capillary column) equipped with a flame ionization detector using chlorobenzene as an internal standard substance. Both the injector and detector temperatures were 523 K, and the column temperature was 443 K. The components of oxygen formed were analyzed by gas chromatography with TCD detector. The products were satisfactorily identified by gas chromatography/mass spectrometry (GC-MS) and compared with authentic standard samples. Mass balances were verified.

Acknowledgements

References

1 S. Guo, Z. Du, S. Zhang, D. Li, Z. Li and Y. Deng, Green Chem., 2015, **280**, 670–676.
2 C. Shen, Y. J. Wang, C. Dong and G. S. Luo, Chem. Eng. J., 2014, **235**, 75–82.
3 M. Anilkumar and W.F. Hoelderich, Appl. Catal. B: Environ., 2015, **165**, 87–93.
4 H. Ichihashi and H. Sato, Appl. Catal. A: Gen., 2001, **221**, 359–366.

5   Z. Wang, H. Ling, J. Shi, C. Stampfl, A. Yu, M. Hunger and J. Huang, J. Catal., 2018, **358**, 71–79.

6   A. Thangaraj, S. Sivasanker and P. Ratnasamy, J. Catal., 1991, **131**, 94–400.

7   R. Chen, H. Mao, X. Zhang, W. Xing and Y. Fa, Ind. Eng. Chem. Res., 2014, **53**, 6372–6379.

8   R. Prasad and S. Vashisht, J. Catal., 1996, **161**, 373–376.

9   W. Zhong, T. Qiao, J. Dai, L. Mao, Q. Xu, G. Zou, X. Liu, D. Yin and F. Zhao, J. Catal., 2015, **330**, 208–221.

10 P. Serna, M. Lopez-Haro, J. J. Calvino and A. Corma, J. Catal. 2009, **263**, 328-334.

11 P. Rubio-Marqués, J. C. Hernández-Garrido, A. Leyva-Pérez and A. Corma, Chem. Commun., 2014, **50**, 1645-1647.

12 F. Cavani, N. Ballarini and S. Luciani, Top. Catal., 2009, **52**, 935–947.

13 J. S. Reddy and A. Sayari, Appl. Catal. A, 1995, **128**, 231–242.

14 R. Joseph, T. Ravindranathan and A. Sudalai, Tetrahedron Lett., 1995, **36**, 1903–1904.

15 G. Náray-Szabó and L. T. Mika, Green Chem., 2018, **20**, 2171–2191.

16 J. N. Armor, E. J. Carlson, R. Riggitano, J. Yamanis and P. M. Zambri, J. Catal., 1983, **83**, 487–490.

17 K. Rakottyay and A. Kaszonyi, Appl. Catal. A: Gen., 2009, **367**, 32–38.

18 W. Zhong, L. Mao, W. Yi, S. R. Kirk, D. Yin, A. Zheng and H. Luo, Catal. Commu., 2014, **56**, 148–152.

19 S. Liu, K. You, J. Jian, F. Zhao, W. Zhong, D. Yin, P. Liu, Q. Ai and H. Luo, J. Catal., 2016, **338**, 239–249.

20 S. K. Klitgaard, K. Egeblad, U. V. Mentzel, A. G. Popov, T. Jensen, E. Taarning, I.S. Nielsen and C.H. Christensen, Green Chem., 2008, **10**, 419–423.

21 S. Liu, K. You, J. Song, R. Deng, F. Zhao, P. Liu, Q. Ai and H. Luo, Appl. Catal. A: Gen., 2018, **568**, 76–85.

22 K. Suzuki, T. Watanabe and S. I. Murahashi, Angew. Chem. Int. Ed., 2008, **47**, 2079–2081.

23 L. Dong, Y. Xin, X. Liu, Y. Guo, C.-W. Pao, J.-L. Chen and Y. Wang, Green Chem., 2019, **21**, 3081–3090.

24 I. Nowak and M. Ziolek, Chem. Rev., 1999, **99**, 3603–3624.

25 K. Nakajima, J. Hirata, M. Kim, N. K. Gupta, T. Murayama, A. Yoshida, N. Hiyoshi, A. Fukuoka and W. Ueda, ACS Catal., 2018, **8**, 283–290.

26 Md. N. Rashed, S. M. A. H. Siddiki, Md. A. Ali, S. K. Moromi, A. S. Touchy, K. Kon, T. Toyao and K. Shimizu, Green Chem., 2017, **19**, 3238–3242.

27 M. Ziolek, I. Sobczak, P. Decyk, I. Nowak and J. Kujawa, Micropor. Mesopor. Mat., 2000, **35–36**, 195–207.

28 P. Carniti, A. Gervasini, C. Tiozzo and M. Guidotti, ACS Catal., 2014, **4**, 469–479.

29 X. Kong, Y. Zhu, Z. Fang, J. A. Kozinski, I. S. Butler, L. Xu, H. Song and X. Wei, Green Chem., 2018, **20**, 3657–3682.

30 M. Ziolek, I. Sobczak, P. Decyk, K. Sobańska, P. Pietrzyk and Z. Sojka, Appl. Catal. B: Environ., 2015, **164**, 288–296.

31 Y. Fan, S. Cheng, H. Wang, D. Ye, S. Xie, Y. Pei, H. Hu, W. Hua, Z. H. Li, M. Qiao and B. Zong, Green Chem., 2017, **19**, 2174–2183.

32 D. Zhao, J. Feng, Q. Huo, N. Melosh, G. H. Fredrickson, B. F. Chmelka and G. D. Stucky, Science, 1998, **279**, 548–552.

33 Z. Zhao, X. Gao and I. E. Wachs, J. Phys. Chem. B, 2003, **107**, 6333–6342.

34 G. W. Graham, W. H. Weber, C. R. Peters and R. Usmen, J. Catal., 1991, **130**, 310–313.

35 L. J. Burcham, J. Datka and I. E. Wachs, J. Phys. Chem. B, 1999, **103**, 6015.

36 J. M. Jehng and I. E. Wachs, Chem. Mater., 1991, **3**, 100–107.

37 A. A. Gabrienko, S. S. Arzumanov, A. V. Toktarev, I. G. Danilova, I. P. Prosvirin, V. V. Kriventsov, V. I. Zaikovskii, D. Freude and A. G. Stepanov, ACS Catal., 2017, **7**, 1818–1830.

38 P. R. H. P. Rao, A. V. Ramaswamy and P. Ratnasamy, J. Catal., 1992, **137**, 225–231.

39 A. M. Prakash and Larry Kevan, J. Am. Chem. Soc., 1998, **120**, 13148–13155.

40 B. Kilos, A. Tuel, M. Ziolek and J. C. Volta, Catal. Today, 2006, **118**, 416–424.

41 K. Peng, X. Li, X. Liu and Y. Wang, Mol. Catal., 2017, **441**, 72–80.

42 N. E. Thornburg, A. B. Thompson and J. M. Notestein, ACS Catal., 2015, **5**, 5077–5088.

43 L. Kong, C. Zhang, J. Wang, W. Qiao, L. Ling and D. Long, Sci. Rep., 2016, **6**, 21177.

44 I. D. Ivanchikova, N. V. Maksimchuk, I. Y. Skobelev, V. V. Kaichev and O. A. Kholdeeva, J. Catal., 2015, **332**, 138–148.

45 C. García-Sancho, I. Sádaba, R. Moreno-Tost, J. Mérida-Robles, J. Santamaría-González, M. López-Granados and P. Maireles-Torres, ChemSusChem, 2013, **6**, 635–642.

46 Z. Yan, L. Fu, X. Zuo and H. Yang, Appl. Catal. B: Environ., 2018, **226**, 23–30.

47 D. T. Bregante, N. E. Thornburg, J. M. Notestein and D. W. Flaherty, ACS Catal., 2018, **8**, 2995–3010.

48 A. Takagaki, J. N. Kondo, M. Hara, S. Hayashi and K. Domen, Chem. Mater., 2005, **17**, 2487–2489.

49 T. Barzetti, E. Selli, D. Moscotti and L. Forni, J. Chem. Soc., Faraday Trans., 1996, **92**, 1401–1407.

50 S. Ghosh, S. S. Acharyya, R. Tiwari, B. Sarkar, R. K. Singha, C. Pendem, T. Sasaki and R. Bal, ACS Catal., 2014, **4**, 2169–2174.

51 A. Tabler, A. Häusser and E. Roduner, J. Mol. Catal. A: Chem., 2013, **379**, 139–145.

52 L. Lin, Z. K. Yang, Y. F. Jiang and A. W. Xu, ACS Catal., 2016, **6**, 4449–4454.

53 J. Li, G. Liu, X. Long, G. Gao, J. Wu and F. Li, J. Catal., 2017, **355**, 53–62.

54 T. Matsushima, Surf. Sci., 1985, **157**, 297–318.

55 S. Han and C. B. Mullins, ACS Catal., 2018, **8**, 3641–3649.

56 G. Qiu, C. Huang, X. Sun and B. Chen, Green Chem., 2019, **21**, 3930–3939.

57 G. K. Koyanagi, D. Caraiman, V. Blagojevic and D. K. Bohme, J. Phys. Chem. A, 2002, **106**, 4581–4590.

58 M. C. Silaghi, C. V. Aleix and C. Copéret, ACS Catal., 2016, **6**, 4501–4505.

59 C. Tiozzo, C. Bisio, F. Carniato, A. Gallo, S. L. Scott, R. Psaro and M. Guidotti, Phys. Chem. Chem. Phys., 2013, 15, 13354–13362.

60 P. D. Patel, B. B. Laird and W. H. Thompson, J. Mol. Catal. A: Chem., 2016, **424**, 1–7.

61 H. Zhai, X. Zhang, W. Chen, X. Huang and L. Wang, J. Am. Chem. Soc., 2011, **133**, 3085–3094.

62 W. Yan, A. Ramanathan, P. D. Patel, S. K. Maiti, B. B. Laird, W. H. Thompson and B. Subramaniam, J. Catal., 2016, **336**, 75–84.

63 X. Jin, C. Lv, X. Zhou, C. Zhang, Q. Meng, Y. Liu and G. Chen, Appl. Catal. B: Environ., 2018, **226**, 53–60.

64 A. Corma, P. Concepción and P. Serna, Angew. Chem. 2007, **119**, 7404-7407.

65 M. Trejda, A. Tuel, J. Kujawa, B. Kilos and M. Ziolek, Micropor. Mesopor. Mat., 2008, **110**, 271–278.

66 C. Lee, W. Yang and R. G. Parr, Phys. Rev. B: Condens Matter Mater. Phys., 1988, 37, 785–789.

67 S. Grimme, J. Antony, S. Ehrlich and H. Krieg, J. Chem. Phys. 2010, 132, 154104-154119.

68 K. Fukui, Acc. Chem. Res., 1981, 14, 471–476.

Figure-abstract